

# SNOWPACK PROPERTIES IN DRONNING MAUD LAND, ANTARCTICA, COMPARED TO ENVISAT ASAR AND SCATTEROMETER MEASUREMENTS

G. Rotschky<sup>(1)</sup>, W. Rack<sup>(1)</sup>, H. Oerter<sup>(1)</sup>

<sup>(1)</sup> Alfred Wegener Institute for Polar and Marine Research, D-27515 Bremerhaven,  
P.O.Box 120161, Germany  
Email: grotschky@awi-bremerhaven.de

## INTRODUCTION

The knowledge of the Antarctic mass balance and its spatial and temporal variability is still insufficient for determining the ice sheet's contribution to global sea level rise with high accuracy [3]. We aim at extending previous studies to combine backscatter information over Antarctica in order to classify regions with similar backscattering nature and therefore snow pack properties. This information is used to derive better estimates of snow accumulation rates by means of SAR for the Dronning Maud Land area (Fig.1). In contrast to Synthetic Apertur Radar (SAR), spaceborne scatterometers give valuable information on backscattering characteristics at low spatial but high temporal resolution, providing a whole set of different looking and incidence angles on a certain ground location.

In general, microwave signatures depend on absorption and scattering losses within the firn pack [11]. Previous authors linked the azimuthal modulation of the measured signal amplitude (backscattering anisotropy) with the orientation of surface roughness features, such as sastrugi, for interfering the wind field over ice sheets [10, 14]. The minimum of the backscatter versus azimuth direction was found to generally correspond to the wind direction. Image time series and frequency difference images (Ku and C band) have been applied over Greenland to extract snow and ice facies [4, 9], separating the higher elevation dry snow zone from the percolation and wet snow zone near the coast. The snow accumulation rate is seen as a key factor, determining physical snow and firn properties, like layering, grain size and density, thus controlling the backscattering mechanism. Spatiotemporal variations in snow deposition conditions can thus be expected to have a major impact on the sensed backscatter coefficient. The capability of microwave remote sensing for estimating snow accumulation has been recognized, due to the reported inverse correlation between backscattering coefficient  $\sigma^0$  and accumulation rate within the dry snow zone [2, 5, 9, 10].

Our approach is the combination of overlapping scatterometer images at different frequencies to define snow pack classes by three parameters for Dronning Maud Land (DML), Antarctica. Within such defined snow regimes the relationship between SAR backscattering and snow pack properties, in the first place accumulation rates derived by stake readings, is investigated. This is done along a traverse route from the German Neumayer base (70°39'S, 08°15'W) at the ice shelf Ekströmisen to the German base camp Kottas (74°12'S, 9°44'W).

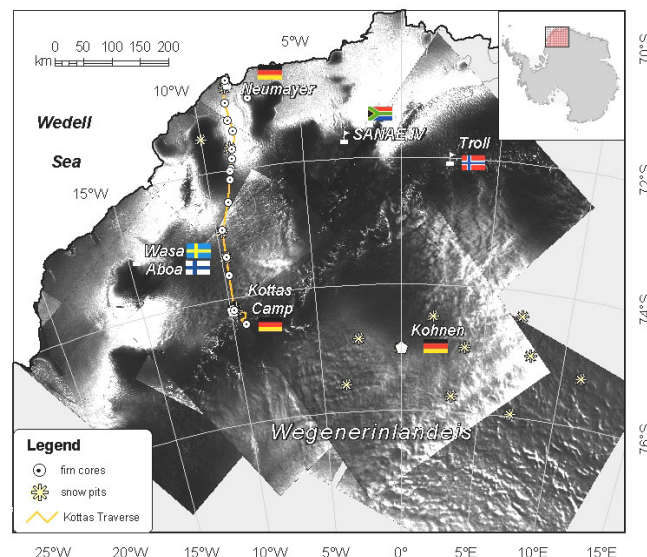


Fig.1. Envisat ASAR mosaic of Dronning Maud Land study region, showing the Kottas-traverse route connecting the German bases Neumayer (70°39'S, 08°15'W) and Kottas camp (74°12'S, 9°44'W) as well as snow pit and firn core sampling sites

## DATA AND METHODS

We used VV-polarized 5.3 GHz (C band) Escat and overlapping 14.3 GHz (Ku band) Nscat data, acquired during austral winter weeks in 1997 to characterize backscattering properties of the Antarctic ice sheet. During this time, the upper snow layers are completely dry. Thus the ice cap holds stable conditions during our imaging time interval. The Escat sensor (ERS-2 Active Microwave Instrument in wind scatterometer mode) measures the surface backscattering  $\sigma^0$  with three right-looking antenna over a single 500 km-wideswath to a southernmost extent of 79.5°S, and with a nominal resolution of 50 km [1]. The Nscat instrument onboard ADEOS-1 overlaps two 600-km-wide swaths on both sides of the satellite track, separated by a 400 km gap. 6 VV- and 2 HH-polarized antenna beams cover the Antarctic ice sheet to within 1.2° of the pole. Despite of the short mission duration (September 1996 to June 1997), the Nscat time series enable more detailed studies of the surface's electromagnetic scattering properties, due to its higher spatial resolution of 25 km and broader azimuth and incidence angle coverage. For each sensor data of a full repeat pass cycle were combined and bound into a polar-stereographic grid with a pixel spacing of 25 km. Thus the acquisition time interval includes 35 days for Escat and 41 days for Nscat. The single beam measurements were allocated in grid cells, using a simple drop in the bucket method. The number of passes included in each image grid cell varies according to the satellites swath geometry in relation to the grid cell location. Towards the southern imaging limit the number of incidence angles decreases, e.g. for Escat, southward 78.8°S no incidence angles less than 30° are available.

Following [13] and [16], three slightly modified parameters have been calculated for each grid cell in order to characterize the backscattering: the mean backscattering coefficient  $\sigma_{\text{mean}}^0$  within the incidence-angle range of 30 to 40 degrees over all viewing angles  $\alpha$ , the factor of anisotropy ( $FA$ ), and the incidence angle gradient ( $IG$ ). The latter was evaluated by applying a linear fit over all  $\sigma^0$  measurements within the incidence angle range of 20°-50°.  $FA$  describes the azimuthal modulation of  $\sigma^0$  and is calculated according to (1)

$$FA = \frac{\sum_{j=1}^{18} |\sigma_{\Delta\alpha_j, \text{mean}}^0 - \sigma_{\text{mean}}^0|}{\sigma_{\text{mean}}^0} \quad \alpha_j = 20 \cdot j, \Delta\alpha_j = \alpha_{j-1} \dots \alpha_j \quad (1)$$

where  $\Delta\alpha_j$  stands for 18 azimuth angle groups in 20° steps. This way we received three images for each sensor, respectively, mapping the spatial distribution of backscattering characteristics over the ice sheet. They were linearly scaled and stretched to 8-bit channels, and used as input for a Maximum Likelihood classification. Signature values for 10 classes were forced by training areas, that were chosen after first applying an unsupervised K-Means classification to our data in order to identify areas with pronounced backscattering behaviour.

Envisat ASAR wideswath data, acquired in 2004, were geocoded using the RAMP Digital Elevation Model [8]. Calibration and gridding to a 100 m raster was accomplished, using the Gamma Remote sensing software package. The result was then filtered by applying a 3x3 running mean. The  $IG$  derived from Escat data was used to normalize the ASAR data to an incidence angle of 35°. Because  $FA$  is low in this area, no correction was applied for the anisotropy of backscattering. Various ground truth data are available, collected by the Alfred Wegener Institute for Polar and Marine Research (AWI). A line of 675 stakes at 500-m interval was set up along the Neumayer - Kottas Camp traverse route (Fig.1), providing a transect of mass balance information through the DML region of high spatial resolution for the period 1999-2001. Here we correlate accumulation data from snow pit studies and stake line readings with satellite data.

## RESULTS

### Frequency dependent Backscattering Differences

$\sigma_{\text{mean}}^0$  (Nscat) was compared to  $\sigma_{\text{mean}}^0$  (Escat) along the transect from Neumayer station on the Ekström ice shelf to the Kottas base camp (Fig.2). Topographic information was taken from the RAMP Digital Elevation Model [8]. From the grounding line, 120 km south of Neumayer, the ice sheet is rising in steps from the flat ice shelf area to the high elevation polar plateau (2000 m a.s.l.). Interestingly, the boundary between the coastal percolation to the dry snow zone is marked by the sudden disjunction of our scatterometer profiles. Within regions effected by summer melt, buried ice lenses and hoar layers act as strong scatterers and prevent microwaves independently of frequency from deeper penetration into the snow pack. Further upslope (elevation above 400 m a.s.l.), where mean annual air temperatures do not exceed -10°C [9], frequency differences in backscattering response start to come out. The cross over to dry snow conditions with increasing altitude goes along with a remarkable drop in backscattering coefficient  $\sigma_{\text{mean}}^0$  from -2 dB to -10 dB (Escat) and accordingly -7 dB (Nscat). Such phenomena has been utilized by [4] to distinguish snow facies on the Greenland ice sheet. Within the dry snow zone higher absorption losses within the snow pack, due to a higher

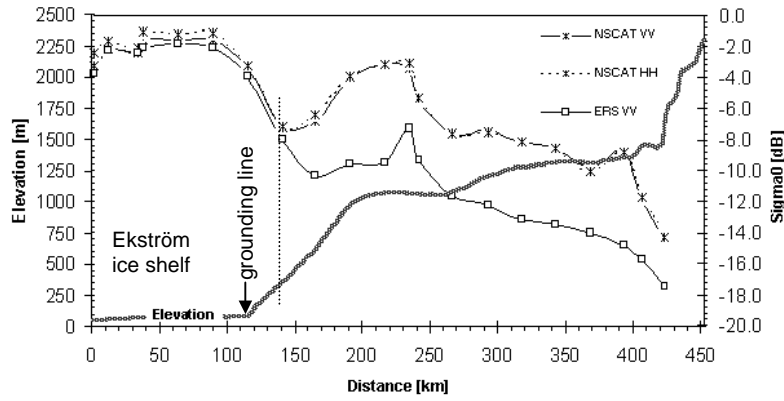


Fig.2.  $\sigma_{\text{mean}}^{\circ}$  along the traverse route between Neumayer station and Kottas Camp

C band penetration depth are causing generally lower  $\sigma^{\circ}$  values for Escat, but both curves progress parallel, with a frequency differences of up to 6.2 dB. A notable sudden rise in backscattering between km 150-250 can be observed for both wavelengths, but is less pronounced for the longer wave ERS data. A comparison with accumulation measurements suggests, that a low net mass balance within this range of our transect might cause changes in grain size and layering in an order, that is primarily effecting the shorter wave Ku band. The Nscat  $\sigma^{\circ}$  is almost independent of frequency which was also observed in Greenland [17].

### Snow Pack Classification

Applying a Maximum Likelihood classification to our C and Ku band data by combining images of  $\sigma_{\text{mean}}^{\circ}$  ( $30^{\circ} \leq \theta \leq 40^{\circ}$ ), *IG* and *FA*, regions of comparable backscatter response could be delimited for the Antarctic ice sheet. The resulting pattern for DML, derived from Escat measurements is shown in Fig.3. The spatial variability in observed parameters is reflecting differences in snow pack characteristics like the surface roughness, density, layering or grain size [13]. The results yield a similar general pattern of surface classes for both VV polarized scatterometer data. Thus we consider this simple method as robust for mapping different polar snow facies. The higher resolution Nscat sensor enables a more detailed discrimination of the single classes shape and extent. For all excluded classes the backscattering level of Escat is generally reduced compared to the Nscat observations, due to differences in penetration depth and absorption loss within the snow pack. At the same time, the Escat data generally exhibits higher values for *FA*, than those observed for the Nscat data, excepting class 6, which distribution does fairly match with the Nscat result.

For DML snow surface classes reflect variable surface conditions. This is due to spatially variable weather conditions, wind fields, and accumulation rates [12, 15], governed by orographic effects and surface undulations. In agreement for both frequencies, regions presenting extreme values in one or more of our input parameters stand out clearly. Class 1 is represented by a bright band of extremely high  $\sigma_{\text{mean}}^{\circ}$  (up to 0 dB) at the margins of the continent, where effects of rapid grain growth and formation of ice lenses and pipes near the surface during the summer months combine to form strong scattering layers. Little *FA* and *IG*, together with only small frequency differences between Nscat and Escat indicate, that here near surface scattering is the dominant mechanism. In opposite, for regions with fine-grained firm within the dry snow zone the penetration depth is in the order of a few hundred times the wavelength [2].

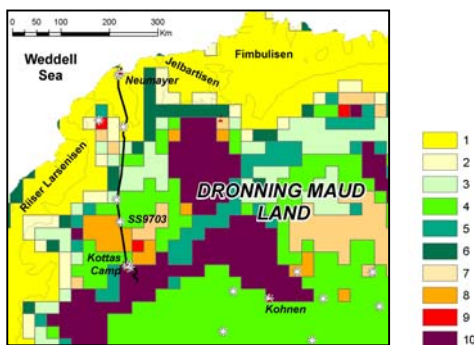


Fig.3. Classification result (Escat), for classes see table 1

Table 1. Escat Maximum Likelihood cluster means

Class	$\sigma^{\circ}$	<i>FA</i>	<i>IG</i>
1	-3.139	0.094	-0.153
2	-6.060	0.284	-0.135
3	-9.946	0.305	-0.173
4	-11.470	0.398	-0.174
5	-10.076	0.345	-0.352
6	-7.870	0.129	-0.189
7	-10.609	0.603	-0.221
8	-14.518	0.565	-0.336
9	-12.699	0.881	-0.160
10	-18.319	0.251	-0.324

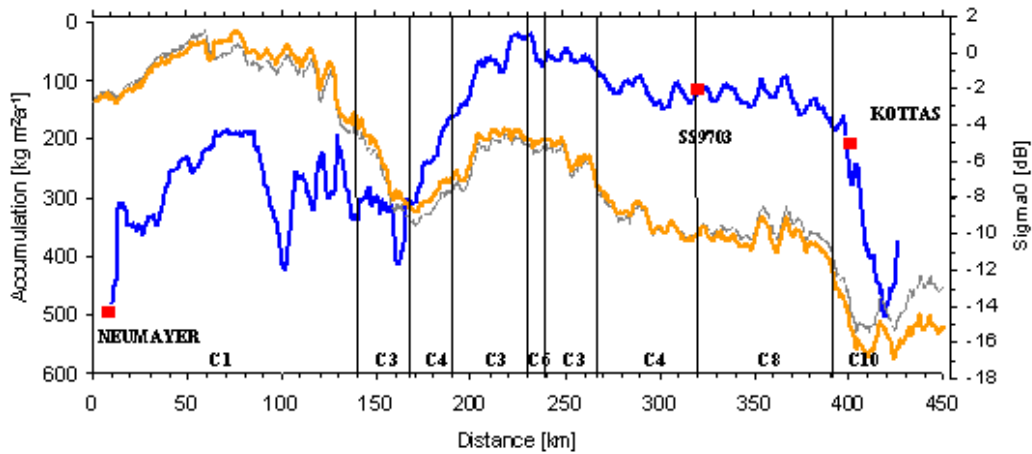


Fig.4. Five-year mean net snow accumulation derived from stake readings along the Kottas-traverse route for the time period 1997-2001 (blue), inversely plotted against normalized (orange) and unnormalized (grey) ASAR  $\sigma^0$ . Red squares mark the location of snow pits, described in the text.

Here, absorption losses cause low values of  $\sigma^0_{\text{mean}}$ . They are represented by class 10, which is furthermore characterized by high  $FA$  and low  $IG$ . Regions of strong katabatic air flow, which is causing a higher surface roughness, are represented by classes 7, 8, and 9, characterized by significantly increased values for  $FA$ . The dependence of this parameter on wind-generated erosional and depositional features, i.e. sastrugi [10, 14] and snow dunes is well known [7]. In DML major snow redistribution of such kind is affected by the Ritscherflya mountain ranges [15]. We hold various ground truth data, crossing from the coastal percolation zone to the dry snow zone on the polar plateau. With these we can link our snow pack classes derived by satellite data and answer questions on their morphological differences.

#### Accumulation vs. ASAR Backscattering Cross Correlation

The normalized ASAR data show a remarkable inverse relationship to the average snow accumulation (Fig.4). Traceable is the typical trend of decreasing snow accumulation with increasing elevation and distance to the coast [15]. A section of strong variations can be observed from km 90-170 along the rise from the grounded coastal areas (also Fig.2). Near Kottas mountains, the local terrain and wind field is causing a sudden rise in net snow accumulation, reaching values up to  $500 \text{ kg m}^{-2} \text{ a}^{-1}$ . A varying snow accumulation can be related with changes in snow pack properties, especially the layer thickness and the grain size-depth profile. Such changes are mirrored by the corresponding surface backscattering signatures, which show a clear increase in  $\sigma^0$  with decreasing snow accumulation, as observed earlier by Antarctic and Greenland ice sheet studies [2, 4, 5, 9, 18]. However no exclusive dependence between accumulation and  $\sigma^0$  can be seen over the entire spectrum of crossed snow pack classes.

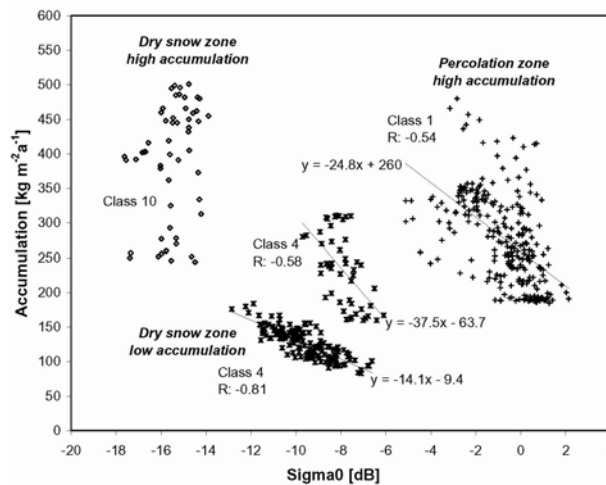


Fig.5. Scatterplot of ASAR wide swath  $\sigma^0$  vs. stake line net accumulation rates

Comparable average accumulation rates can cause backscattering responses on different levels, depending on snow pack properties. Based on a map of snow classes (Fig.3), resulting from the Escat classification, we studied the accumulation versus  $\sigma^0$  correlation separately for individual classes. Examples for this are shown in Fig.5. Percolation zone measurements separate here as a cluster of rather scattered points on the right side, exhibiting a correlation factor R of  $-0.54$ . Within this zone  $\sigma^0$  is generally higher, than within the dry snow zone. Snow pit studies near Neumayer station show, that high summer temperatures alter the snow pack in a way, that contributes to stronger backscattering response. The snow was described as coarse-grained material, containing a series of up to 2 cm thick ice lenses. A mean density of  $0.42 \text{ kg m}^{-3}$  was found within the snow pack's upper 2 m.

No correlation was observed in class number 10 near the Kottas Mountains, where local effects cause spatially highly variable accumulation rates, which cannot be resolved in the classification procedure by scatterometer data. A correlation between  $\sigma^0$  and accumulation of up to  $-0.81$  can be found for low accumulation areas within the dry snow zone, covered by class number 4. Snow pit SS9703 reveals for this class a series of alternating high-density layers of fine grains and lower density, coarse-grained firn, caused by annual and seasonal varying wind and temperature conditions. Additionally wind crust of less than 1 mm thickness are found at several depths. Our findings are consistent with a previous study [5], that found backscattering to be generally more sensitive to changes in accumulation when the accumulation rate is low.

## SUMMARY AND CONCLUSION

We used Escat and Nscat scatterometer data in order to identify polar regions with similar backscattering and therefore snow pack properties by 3 parameters ( $\sigma^0_{\text{mean}}$ , azimuth and incidence angle dependence of backscattering *FA* and *IG*). Strong variations are observed across the Antarctic ice sheet. The classification of both sensors is similar, showing that Escat is a useful tool to characterize the snow pack backscattering, despite a limited imaging geometry. Differences can be explained by the higher penetration depth in C-band and the larger contribution of volume scattering. Envisat ASAR wide-swath data from a test site in Dronning Maud Land were normalized using *IG* and neglecting the mostly small anisotropy in this area. Our hypothesis, that in the same classified regions a good correlation exists between accumulation and backscattering amplitude, is only partly confirmed by the normalized ASAR data. The assumption was tested along a continuous 400 km long accumulation profile. At least in one class, the reason may be strong orographic effects near the Kottas mountain range. Because ASAR wide-swath data are regularly acquired and backscattering in the dry snow zone is quite stable, staggings of many scenes over several years will be used in the future to reduce the speckle. Also the normalization procedure may allow to average scenes with different imaging geometry, even from the ascending and descending pass.

Not all surface classes are represented in the test area, and ground truth is not available for all surface classes. Future snow stratigraphy studies and firn core drillings should concentrate on those areas to establish better accumulation-backscattering relations for such snow classes. With regard to Ku-Band and altimetry missions, more attention should be paid to snow grain size [6]. With the gained experience some of the initial classes for the MLC algorithm can be redefined to cluster the solution of the classification around well known snow classes. The classification result and the stability of surface classes will be of interest for oncoming Cal/Val activities for Cryosat, to be launched in March 2005, and for the planning of snow and accumulation studies of future ITASE (International Trans-Antarctic Scientific Expedition) campaigns.

## REFERENCES

- [1] E.P.W. Attema, "The active microwave instrument on-board the ERS-1 satellite", *Proc. IEEE*, vol.79, pp. 791–799, June 1991.
- [2] A.W. Bingham, and M. Drinkwater, "Recent changes in the microwave scattering properties of the Antarctic ice sheet", *IEEE Trans. Geosci.Remote Sens.*, vol. 38, pp. 1810–1820, July 2000.
- [3] J.A. Church, K.M. Gregory, P. Huybrechts, M. Kuhn, C. Lambeck, M.T. Nhuan, D. Qin, P.L. Woodworth, "Changes in sea level", in: *Climate Change 2001: The Scientific Basis: Contribution of Working Group I to the Third Assessment Report of the Intergovernmental Panel on Climate Change*, J.T. Houghton, Y. Ding, D.J. Griggs, M. Noguer, P.J. Van der Linden, X. Dai, K. Maskell and C.A. Johnson, Eds. Cambridge, New York: Cambridge University Press, pp. 639-694, 2001.
- [4] M.R. Drinkwater, D. G. Long, and A.W. Bingham, "Greenland snow accumulation estimates from satellite radar scatterometer data", *J. Geophys. Res.*, vol. D24, pp. 33,935–33,950, December 2001.
- [5] R. Forster, K.C. Jezek, J. Bolzan, F. Baumgartner, and S. P. Gogineni, "Relationships between radar backscatter and accumulation rates on the Greenland ice sheet", *Int. J. Remote Sens.*, vol. 20, pp. 3131–3147, 1999.

- [6] M. Gay, M. Fily, C. Genthon, M. Frezzotti, H. Oerter, and J-G. Winther, “Snow grain-size measurements in Antarctica”, *J. Glaciol.*, vol. 48, pp. 527-535, 2002.
- [7] I.D. Goodwin, “Snow accumulation and surface topography in the katabatic zone of Eastern Wilkes Land, Antarctica”, *J. Glaciol.*, vol. 37, pp. 383-387, 1991.
- [8] H. Liu, K. Jezek, B. Li, and Z. Zhao, “Radarsat Antarctic Mapping Project digital elevation model version 2”, Digital media, National Snow and Ice Data Center, Boulder, CO, USA, 2001.
- [9] D.G. Long, and M. R. Drinkwater, “Greenland ice-sheet surface properties observed by the Seasat-A scatterometer at enhanced resolution”, *J. Glaciol.*, vol. 40, pp. 213–230, 1994.
- [10] D.G. Long, and M. R. Drinkwater, “Azimuth variation in microwave scatterometer and radiometer data over Antarctica”, *IEEE Trans. Geosci. Remote Sens.*, vol. 38, pp. 1857–1870, July 2000.
- [11] C. Mätzler, “Applications of the interaction of microwaves with the natural snow cover”, *Remote Sens. Rev.*, vol. 2, pp. 259–392, 1987.
- [12] H. Oerter, F. Wilhelms, F. Jung-Rothenhäusler, F. Göktas, H. Miller, W. Graf, and S. Sommer, “Accumulation rates in Dronning Maud Land as revealed by dielectrical-profiling measurements at shallow firn cores”, *Ann. Glac.*, vol. 30, pp. 27–34, 2000.
- [13] W. Rack, “Streuverhalten und Morphologie der Antarktischen Schneedecke aus Scatterometer-Messungen von ERS-1”, Ph.D. dissertation, Univ. Innsbruck, Innsbruck, Austria, 1995.
- [14] F. Rémy, M. Ledroit, and J. F. Minster, “Katabatic wind intensity and direction over Antarctica derived from scatterometer data”, *Geophys.Res. Lett.*, vol. 19, pp. 1021–1024, 1992.
- [15] C. Richardson-Näslund, “Spatial characteristics of snow accumulation in Dronning Maud Land, Antarctica”, *Global and Planetary Change*, vol. 42, pp. 31-43, 2004.
- [16] H. Rott, and W. Rack, “Characterization of Antarctic Firn by Means of ERS-1 Scatterometer Measurements”, in: *Proceedings of International Geoscience and Remote Sensing Symposium, 10-14 July 1995, Florence, Italy*, IEEE Publications, vol. 3, pp. 2041-2043, 1995.
- [17] C.T. Swift, P.S. Hayes, J.S. Herd, W.L. Jones, and V.E. Delnore, “Airborne microwave measurements of the Southern Greenland ice sheet”, *J. Geophys. Res.*, vol. 90, pp. 1983-1994, 1985.
- [18] V.R. Wismann, and K. Boehnke, “Monitoring snow properties on Greenland with ERS scatterometer and SAR”, *Eur. Space Agency Spec. Publ.*, *ESA SP-414*, 857–862, 1997.